Evaluating quality of marquetries by applying active IR thermography and advanced signal processing

Evaluating quality of marquetries by applying active IR thermography and advanced signal processing

A.O. Chulkov [1], S. Sfarra [2*, 1], N. Saeed [3], J. Peeters [4, 5], C. Ibarra-Castanedo [6], G. Gargiulo [7], G. Steenackers [4], X.P.V. Maldague [6], M.A. Omar [3], V. Vavilov [1]

[1] Tomsk Polytechnic University, Lenin Av., 7, 634050, Tomsk, Russia

[2] Department of Industrial and Information Engineering and Economics (DIIIE), University of L'Aquila, Piazzale E. Pontieri 1, 67100, Monteluco di Roio – L'Aquila (AQ), Italy

[3] Industrial and Systems Engineering Department, Khalifa University of Science and Technology, 54224, Abu Dhabi, United Arab Emirates

[4] Op3Mech, University of Antwerp, Groenenborgerlaan 171, B-2020, Antwerp, Belgium

[5] Qinetiq Space, Hogenakkerhoekstraat 9, 9150, Kruibeke, Belgium

[6] Computer Vision and Systems Laboratory, Electrical and Computer Engineering Department, Laval University, 1065 av de la Medecine, G1V 0A6, Quebec, Canada

[7] Individual Company of Restoration (Gianfranco Gargiulo), Via Tiberio 7b, 80073, Capri (NA), Italy

[*] stefano.sfarra@univaq.it

Abstract: Marquetry method is important in the culture of the Italian community as can be witnessed from the large quantity of artworks that have been realized in this way. The monitoring of the integrity of such pieces poses a great challenge given the need of a reliable and nondestructive technique able to detect surface and subsurface defects. In this work, two ancient marquetry samples containing natural defects were inspected thanks to active thermography by using time-tested, safe and resilient advanced signal processing algorithms (*i.e.*, principal component thermography, correlation contrast, pulsed phase Fourier transform amplitude and phase, cold image subtraction contrast, and polynomial fitting). The latter have been applied to provide a 2D map of the defects.

Anyway, in the cultural heritage field, one of the main interest of restorers is the volume of the subsurface defects for structural analyses. The emphasis in this study is placed on the use of dynamic thermal tomography (DTT) as an advanced technique of active thermal non-destructive testing. The main concepts of DTT are illustrated in the manuscript, while a special technique for defect thermal characterization has been used during the second analysis to validate tomographic results. Finally, the position of the main defects retrieved by means of the established techniques applied during the first analysis have been confirmed by DTT.

1. Introduction

The use of infrared (IR) thermographic monitoring for the inspection of cultural heritage objects is gaining more acceptance year by year, being conditioned by the demand for a testing technique which combines structural [1-2] and surface investigations [3-4] in order to provide solid conclusions on the state of conservation of art objects.

Infrared thermography (IRT) monitoring has been used in many cases for the inspection of wooden materials. Thirty years ago, Winfree and James proposed to detect defects in laminated wood used in wind tunnel blades [5], while Wu et al. inspected in 1997 particleboards [6], which are common products in the wood industry [7–8]. The evaluation of different knot diameters in wood specimens was the basis of the research conducted 1998 by Quin Jr. *et al.* with an IR image analysis system [9]; in the same year, Nicolotti and Miglietta applied IR thermography (IRT) in combination with some high-technology instruments (*i.e.*, penetrometers, electrical conductivity meters, sonic and ultrasonic detectors, radar and x ray tomography) to assess wood defects [10]. Thermography for pole inspection (part I) and wood defects detection (part II) was the core of the study conducted by Wyckuyse and Maldague in 2001 [11–12]. In particular, the problem of wood pole nondestructive testing (NDT) was analysed using a dedicated thermal model and three different types of thermal stimulation: internal (through-hole), external, and microwave, while, in the next part of the research, the wood decay inspection problems was treated in a simpler way: the circular geometry was replaced by the flat one, and only shallow defects were considered.

In 2001, Hwang and et al. measured the surface temperature of different wood specimens subjected to longitudinal and lateral compression loading. The relationships between the compression strain/fracture characteristics of the material, and the temperature rise were discussed [13].

Berglind and Dillenz presented results of measurements aimed to evaluate the potentials of pulse thermography (PT) as a method that allows the detection of glue deficiency in laminated wood. In this research, the efficiency of using short observation times was underlined along with the fact that starved glue joints revealed about a half of the temperature signal related to the areas with total lack of glue [14]. Ganne-Chédeville *et al.* studied the influence of welding parameters and wood grain orientation on surface temperature profiles, as well as distribution and final strength of welded connections; in the latter case, nondestructive evaluation was performed by means of IRT, thus allowing the evaluation of maximal and average peak temperature, as well as temperature profiles and rate of temperature elevations [15]. An integrated approach including the use of electronic speckle pattern interferometry (ESPI) and IRT for the evaluation of damage in veneered wood artworks has been undertaken in [16]. IRT was not able to reveal the presence of subsurface defects, such as delaminations and worm galleries, by contrast with the ESPI technique. The latter was found to be suitable to extract the information on the above-mentioned types of defects. However, wood galleries were detected thermographically thanks to the use of advanced post-processing analysis [17]. It was demonstrated that pulsed phase thermography (PPT) and holographic interferometry (HI) are valuable tools for qualitative and quantitative assessment of artworks.

Choi et al. proposed to use a new type of ultrasonic horns characterized by a tuning fork shape in NDT of wood materials. Geometric conditions were optimized by a finite element analysis (FEA). The presence of defects was visualized by an IR imager [18]. Blessley et al. underlined the feasibility of flash thermography (FT) for the examination and conservation of works of art; in particular, it was indicated that IRT can successfully detect wood grains in the situations where the x-ray technique was helpless, although the detection of voids in wood was still questionable [19]. In 2010, Van Dyk and Lemaster developed four heating techniques, namely, defect side heating, back side heating, forced air heating and pulsed IRT, intended for the detection of dents, holes, gouges, and knots. All four techniques have proven to be successful for detecting at least two types of defects [20]. Also in 2010,

Maierhofer et al. explored the use of active IRT methods for one-sided investigation of the structural integrity of building elements up to depth of about 10 cm. It is worth noting that historical masonries have a very heterogeneous structure containing several different materials, including wood [21].

Some aspects of NDT of various wooden components were analysed by Sfarra et al. in 2011, 2012 and 2013 [22–24]. In particular, multilayer samples simulating cultural heritage objects with fabricated and natural defects were analysed by means of optical, thermographic and ultrasonic NDT techniques. The results were arranged into a multidisciplinary approach to define and design the conservation of wooden objects.

In [25], Conde et al. studied the influence of wood density on results of IR thermographic NDT with hidden defect of varying depths and size. Some defects containing moisture, that is typically associated with wood degradation, were also studied to link temperature indications and water content. The same research topic was also considered in [26].

Mulaveesala et al. described the applicability of the transient thermal wave imaging (TWI) method for the inspection of ply wood [27]. This study highlighted the potentials of transient pulsed thermal imaging approach in the detection of hidden defects, while Pervan et al. focused the attention on the energy analysis in hydrothermal processes and NDT of wood, in particular, determination of wood thermal properties [28].

Hoffmann et al. used three types of IR imagers in two long-term measurement periods performed on standardized wooden samples. Neither passive nor active thermographic methods were able to produce significant temperature indications allowing to detect larvae, boreholes or boredust inside of wooden samples. The authors concluded that IR NDT seems to be not appropriate for detecting insect stages or defects in young trees [29]. The conservation of wood in protected buildings was the topic of the research conducted by Morales-Conde et al. in 2013. It was concluded that the combined use of NDT techniques (among which IRT) constitutes an accurate diagnostic tool for on-site inspection of wooden structures and evaluation of their condition (i.e., IRT enabled the quantification of moisture content while the ultrasonic technique detected density loss in areas of the wood with high moisture content) [30]. Liñán *et al.* demonstrated the validity of IRT for the identification of some types of wood and moisture content in wooden structures, while the ultrasonic method detected the various degrees of deterioration and density-loss in areas of the wood with high moisture content [31].

A sample representing a wooden plate with a metallic insert was used to test a novel microwave excitation system for performing IR thermographic inspection. The obtained thermograms showed that there is a temperature increase in a defect area but the non-uniformity of the microwave beam required to process the thermograms by implementing a concept of temperature contrast [32].

López *et* al. focused attention on two types of irregularities in wood: singularities and defects which are regions of disorder affecting wood quality. In this study, potentials and performance of IRT for detecting the above-mentioned subsurface anomalies were analyzed [33].

A comparative analysis of several NDT techniques, including visible imaging, ultraviolet testing, near-infrared reflectography and trasmittography, IRT, holographic interferometry, digital image correlation, laser speckle contrast imaging and ultrasonic testing was performed on two marquetry samples representing arms' coats, in which one sample was a defect free panel, while the second one contained three subsurface flaws and one surface

putty insert added during the manufacturing stage. The preliminary numerical simulations allowed optimization of experimental parameters thus being an indispensable part of the research [34].

The possibility of using the ensemble methods to automatically detect cracks in oak flooring lamellae via ultrasound-excited thermography and a variety of predictor variables has been investigated in [35]. The best ensemble methods reached the average classification accuracy of 0.8 that was close to the authors' manual image classification.

Qiu and Lau overviewed some recently developed tomography approaches based on the using of mechanical and electromagnetic waves for assessing the structural integrity of wooden buildings [36]. The tomographic method has proven to be accurate and reliable.

Garrido et al. proposed a methodology for the automatic detection of moisture areas affecting the surface of construction materials, including wood [37]. The methodology was based on the application of visible image processing techniques adapted to the analysis of IR thermograms by applying image format conversion format and using a geometric filter and a particular thermal criterion.

Laureti et al. described the pulse-compression thermography (PuCT) approach whereby defect detection was optimized while minimizing temperature elevations on paintings made of canvas and wood. The approach used LED heat sources driven by a coded waveform based on a linear frequency modulated chirp signal [38].

Similar IRT studies performed on artworks including wooden support are described in [39–41]. In particular, an independent component thermography (ICT) and pixelwise algorithm for time-derivative of temperature (PATDT) were applied to raw thermograms [39]. In [40–41], the results obtained by means of near-infrared reflectography (NIRR) and IRT were compared and discussed aiming the detection of the largest parts of defects present in different objects of cultural heritage and mock-ups.

At the end of this short review, it is worth mentioning that applications of IR thermographic NDT are continuously broadening in the last decades. This technique has been successfully used for the evaluation of artistic heritage, historic artefacts and archaeological findings [42–43], studies of temperature gradients within samples and furnaces in temperature-modulated differential scanning calorimetry (TMDSC) [44], evaluation of heat loss in buildings [45], detection of defects in aluminium plates [46], diagnosis of mosaics [47] ceramic plates [48], and book-bindings [49].

The use of IRT for inspecting wooden products and art masterpieces is challenging because of an orthotropic nature of wood (i.e., the material properties into the three perpendicular directions – axial, radial, and circumferential – are different). The situation is complicated even more when pieces of wood are put in contact in order to form the so-called marquetry. The marquetry method involves combining a variety of cut and shaped wood-veneer sections (or other materials) of differing colours and sizes to build up a pattern or image in the manner of a jigsaw puzzle. This is then applied to a substrate and fitted to the object to be decorated. Therefore, the marquetry objects to be tested vary significantly by shape, size, structure and thermal properties [50, 51]. Optical stimulation of such objects is difficult to use because of their highly non-uniform thermal patterns characterized by uneven absorption coefficient. Many known algorithms used for enhancing signal-to-noise ratio, such as principal component analysis, correlation contrast, Fourier transform, cold image subtraction contrast, polynomial fitting etc., are bulky and time-consuming and provide only 2D maps of defect indications [52]. In

conservation of cultural heritage, one of the restorers' efforts is the evaluation of subsurface defect volume to use it in further structural analysis [1, 2].

The emphasis in this study is done on the use of *dynamic thermal tomography* (DTT) as an advanced technique of active thermal non-destructive testing [53]. The main concepts of DTT are illustrated in the next section. Also, a special technique of defect thermal characterization has been used to validate tomographic results.

2. Maxigrams and Timegrams (Dynamic Thermal Tomography)

With the term "thermal tomography" the authors specify a procedure that enables slicing a sample for particular depth layers by analysing peculiarities of transient heat conduction in solids. According to the thermal non-destructive testing (TNDT) theory, this is possible only in a one-sided (*front-surface*) test where differential temperature signals experience time retardation with growing defect depth.

The algorithm of *dynamic thermal tomography* (DTT) was proposed by Vavilov and Shiryaev, Tomsk Polytechnic University, Russia, in 1986. For the last decade, this algorithm has been acknowledged by some world Thermal NDT teams. The main idea of DTT is that optimum observation times, i.e., the times when maximum differential temperature signals appear over defects, can be used to characterize defect depths. Therefore, the algorithm allows "slicing" test samples by thin layers with known depth coordinates. A calibration function should be inputted by using theoretical or experimental data (in the ThermoFit Pro® software, the known formula connecting observation times with material diffusivity and defect depth is used). For more details on DTT, the reader may refer to [54–55].

The basic idea is that any dynamic temperature function can be characterized by some specific points in its temporal evolution. In general, this assumption may be applied to any function but, physically, it is related to the temporal behavior of the differential temperature signal $\Delta T(i,j,\tau) = T(i,j,\tau) - T_{nd}(i_{nd}, j_{nd}, \tau)$ defined as a difference between each thermogram point $T(i,j)$ and a chosen reference point $T_{nd}(i_{nd}, j_{nd})$. If a reference point belongs to a non-defect (*nd*) area and some points are located over a subsurface defect, the shape of the $\Delta T(i,j,\tau)$ signal is as shown in Fig. 1.

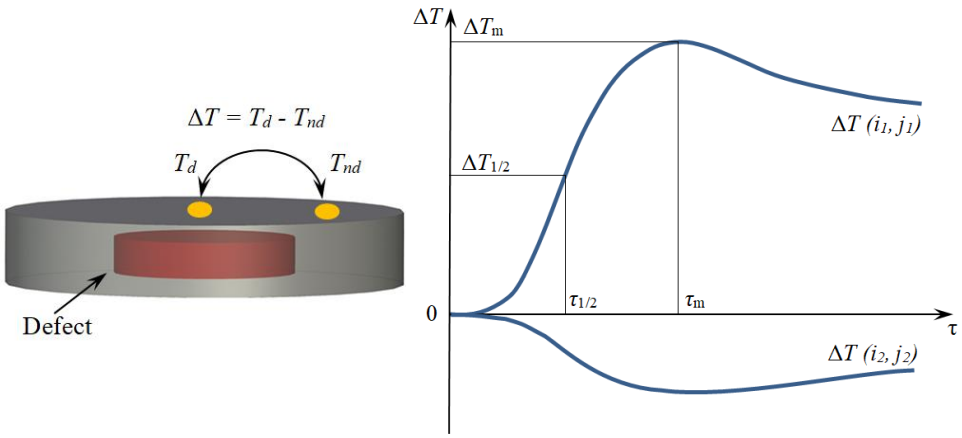

Fig. 1 – Concept of specific heat transit times (maxigrams and timegrams).

A sign of $\Delta T(i, j, \tau)$ signals cab be positive (point i_1,j_1 in Fig. 1) or negative (i_2, j_2) depending on the nature of a defect and its size/location, heating parameters and whether a front or rear surface is monitored. There is a couple of specific points that could be defined in the evolutions shown in Fig. 1. For example, each temperature function of a limited length will reach its extremum value ΔT_m at the time τ_m called *optimum observation time*. The pixel-based pairs of $\Delta T_m(i, j)$ and $\tau_m(i, j)$ values produce *positive* or *negative maxigrams* (ΔT_m -images) and *timegrams* (τ_m -images).

Note that, for example, when determining thermal diffusivity by analyzing a rear-surface temperature response, another pair of specific points is used. Here, they are called *halfgrams* and *timehalfgrams* being related to signals $\Delta T_{1/2} = \Delta T_m / 2$ and times of their appearance $\tau_{1/2}$ (Fig. 1).

Maxigrams exhibit image pixels in their "best" appearance with respect to $\Delta T(\tau)$ signals. Timegrams contain the values of the corresponding heat transit times. In TNDT, maxigrams and timegrams are related to both defect depth and thickness thus allowing defect characterization. However, as mentioned above, these synthetic images could be important in the analysis of various dynamic image sequences (not obligatorily associated with TNDT tests) because they reveal some hidden peculiarities in temporal signal evolutions.

It is important that, due to arbitrary choice of reference points, both *positive* and *negative* temperature signals over defects could appear while determining ΔT signals in a sequence. In a Dirac-pulse (flash) or square-pulse TNDT procedure, temperature signals over defects grow up in time reaching their particular maximums at optimum observation times. These maximums are typically positive, *i.e.*, defect areas are warmer than the background. For a long enough time, due to surface heat exchange and different heat capacity in defect and non-defect areas, some differential temperature signals, in particular, over shallow defects, can become negative and reach other extremum values in their time evolutions but with *opposite* sign. This phenomenon, known in the theory of pulsed TNDT as *signal inversion*, is rarely used in practice because of low amplitudes of inverted signals. However, in periodic heating procedures, both positive and negative extremums appear; moreover, they also might appear in areas of uneven heating. The general theory of temperature signal evolutions is rather sophisticated and omitted in this discussion. The authors limit themselves with the statement that each image pixel can be characterized by the following parameters:

1. ΔT_m^+ is the maximum temperature signal that occurs in a defect area warmer than the background; the corresponding pixel-based values produce the positive maxigram;

2. τ_m^+ is the time when a maximum positive contrast appears; the corresponding pixel-based values produce the positive timegram;

3. ΔT_m^- represents the negative maxigram values;

4. τ_m^- represents the negative timegram values (or time of maximum negative contrast).

Obviously, ΔT_m is zero for all pixels that behave exactly as a chosen reference point. The corresponding τ_m values become indefinite. However, in practice, this takes place only in a reference point itself, because all other points will reveal different ΔT_m values because of noise (non-uniform heating). In a sequence including *S* images, τ_m values are in the range from 1 to *S*. It is important to mention that maxigrams still contain temperature values and represent a kind of synthetic thermograms. Timegrams, in their turn, represent a result of non-linear data conversion, therefore, they cannot be processed statistically in the same way as thermograms and maxigrams. Often, temperature thresholds chosen in maxigrams are used to cut undesirable noise in timegrams.

The necessity of choosing a reference point in thermal tomography is a weak point of this technique, but note that any quantitative evaluation needs a certain type of calibration. In the case of DTT, a general rule is to place the reference close to a suspicious area selected for further analysis but within an area of a relatively uniform temperature. Typically, this can be easily done by the operator although to choose a reference automatically is still challenging.

As follows from the above-mentioned, an image sequence of arbitrary length can be replaced with four synthetic images which contain encoded information on peculiarities of differential signal evolution. In pulsed TNDT, only positive maxigrams and timegrams are typically used. However, if the sample surface temperature varies periodically, both positive and negative timegrams/maxigrams should be analyzed. Positive and negative maxigrams/timegrams may also appear after applying to a source sequence some other algorithms, *e.g.*, normalization, and then processing the modified sequence.

The theory above originates from the analysis of raw temperature signals. Also, it can be applied to processed IR image sequences, for example, normalized. The normalization implements subtracting ambient temperature values from each image pixel and dividing all images in the sequence by a chosen (normalizing)

image, thus dealing with dimensionless (contrast) signals. The maxigram/timegram concept can be also applied to these signals, although the interpretation of obtained results might require further analysis.

Once a timegram is produced, it can be "sliced" by $\tau_m^{(i)} \div \tau_m^{(i+1)}$ intervals. In front-surface TNDT, deeper defects produce longer τ_m values, therefore any particular $\tau_m^{(i)} \div \tau_m^{(i+1)}$ interval corresponds to the respective interval of defect depths $l_1 \div l_2$ (note that τ_m can be expressed either in terms of image numbers or true time). The ThermoFit Pro Program used in this work implements a simple calibration curve that allows converting $\tau_m^{(i)} \div \tau_m^{(i+1)}$ into $l_1 \div l_2$. In the Program, it is possible to perform additional thresholding of "tomograms" by $\Delta T_m \quad (C_m)$ values which are contained in the corresponding maxigram. In this way, the tomograms represent the images where pixels are characterized by τ_m value corresponding to a particular $\Delta T_{m1} \div \Delta T_{m2}$ range. The thermal tomograms obtained on marquetry samples will be discussed below.

5. Marquetry samples: the state of conservation

The marquetries made of fruit woods, have a thickness of about 0.5 mm. They were applied by following the Italian modality called *a buio* (i.e., "at dark") on a solid support (planar and visible beyond the marquetry), also realized in fruit wood (Fig. 2).

a)

b)

Fig. 2 – Marquetries consisting of separate 0.5 mm-thick wooden parts glued on 5 mm wooden base are conventionally called "Boy" (a), and "Girl" (b).

The adhesives used to bind the marquetry on the support are probably of protein origin. The artworks, dating back to the 19th century, have undergone at least two ancient restoration processes, during which, some damaged parts were glued using a different type of adhesive by following inadequate methodologies and thus generating inappropriate results; in addition to this, a dark restoration grout is visible on the support (on the left of the "Boy"). However, the artwork is presented *in patina* ("original painting"). On the wooden tesserae (i.e., under the varnish), a decoration in Indian ink is still clearly visible,

In the "Boy" sample (Fig. 2a), one can reveal some large detachments with deformation inherent to tesserae of the ground and of the arm. The deformation generated a material lift without detachment related to the last part of the belt. In the upper and lower sections of the wood, which represent the background, there are evident dirt crusts. The entire sample surface is covered with a sort of dirt while some residuals of greasy substances are also visible.

As for the "Girl" sample, a lack of tesserae that make up the marquetry is evident on the feet, ground, and left arm (Fig. 2b). These missing areas allow observing the wooden support covered with encrusted dirt and some traces of the old protein glue (which bound the tesserae to the support). On the right side, deformations and lifts with detachments caused a damage of the frame positioned at the perimeter of the marquetry. In the upper part of the wooden background, some dirt crusts are visible. On the right side, as well as on the upper and lower parts of the wooden background, some spots of a different colour are visible. The entire surface is covered with a kind of dirt, while some residuals of greasy substances are also visible.

6. **Testing the** "Boy" and "Girl" samples (flash heating)

This study is related to the detection of some thermal anomalies which can be regarded as defects, such as detachments, lifts, etc., by using one-sided active IRT. The samples were thermally stimulated by means of a Xenon flash tube (optical energy of 3.2 kJ) in a reflection mode from the distance of 1 m, while a FLIR Phoenix IR imager operating into the spectral range of 3-5 μm was used to capture IR thermograms [40].

Below, the test results obtained will be illustrated for the two samples starting from the "Boy". The raw thermogram of Fig. 3a shows some details marked by arrows. In particular, the solid ones (the yellow arrows) indicate subsurface defects while the dotted ones (the brown arrows) point out surface anomalies. The wooden rings and white grouting are the shallowest, while detachments and restorations are the deepest. This is confirmed by using the PPT technique (Figs. 3b, c), in which the deepest anomalies appeared at the frequency of f = 0.0250 Hz (Fig. 3b), while the shallowest were observed at f = 0.1750 Hz (Fig. 3c). Figure 3b adds another detail concerning the right shoulder of the character where a detachment seems to be present. This anomaly was not confirmed by the simple cold image subtraction contrast technique (Fig. 3d), although it clearly appeared by applying the PCT technique, both at the heating (Fig. 3e-h) and cooling (Fig. 3i-l) stages. The area under observation is stressed with the solid yellow arrow.

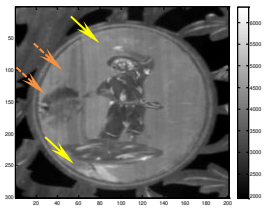

a)

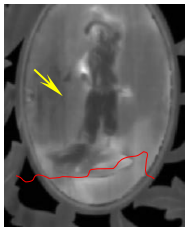

b)

c)

d)

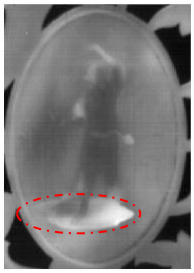

e)

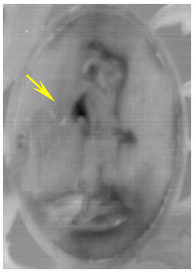

f)

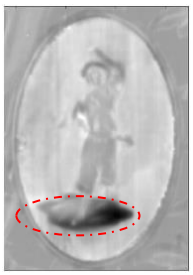

g)

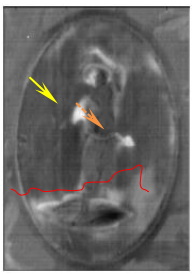

h)

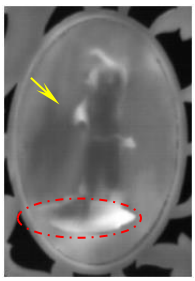

i)

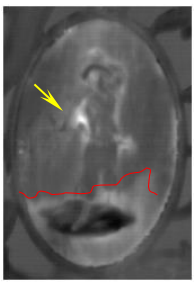

j)

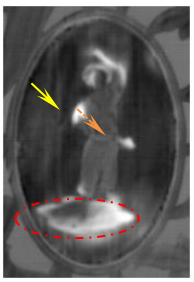

k)

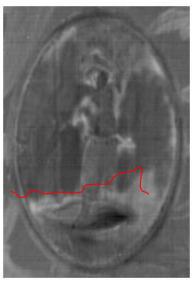

l)

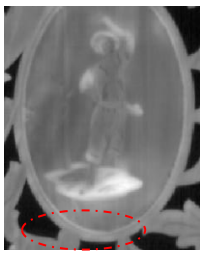

m)

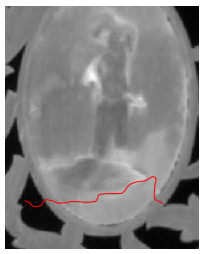

n)

o)

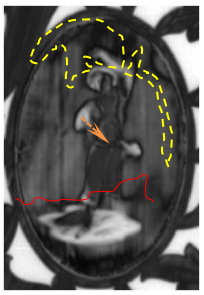

p)

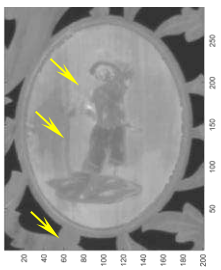

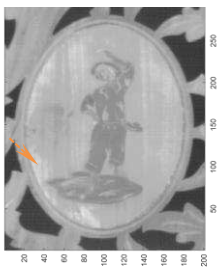

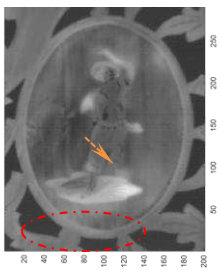

q) *r)* *s)*

Fig. 3 – "Boy" sample: (a) Raw image (time=0.06s), (b) Pulsed phase Fourier transform amplitude (f = 0.0250 Hz), (c) Pulsed phase Fourier transform amplitude (frame = 8, f = 0.1750 Hz), (d) Cold image subtraction contrast (frame = 1024), Heating up phase: (e) PC1 – 7.6%, (f) PC2 – 2.2%, (g) PC3 – 1.1%, (h) PC4 – 0.4%, Cooling down phase: (i) PC1 – 16.7%, (j) PC2 – 3.5%, (k) PC3 – 2.0%, (l) PC4 – 0.5%, (m) Pulse phase Fourier transform phase (frame = 2, f = 0.0250 Hz), (n) Pulsed phase Fourier transform phase (frame = 8, f = 0.1750 Hz), (o) Pulsed phase Fourier transform phase (frame = 232, f = 5.7750 Hz), (p) correlation contrast, and Polynomial fitting (order 4): (q) frame 1, (r) frame 2000, (s) frame 500.

Another thermal anomaly, probably, a detachment, is evident both in the PC1 and PC4 images (see the red dotted oval); in practice, it is inherent to the tesserae composing the ground. The PC1 image exhibits this thermal anomaly when analysing both the heating (Fig. 3e) and cooling (Fig. 3i) stages. Interestingly, the same anomaly also appears after having applied the PPT technique (f = 0.0250 Hz) (Fig. 3m). The PPT phase also shows a particular thermal anomaly located in the bottom part of the marquetry (f = 0.1750 Hz, Fig. 3n) marked with the irregular red line. In the latter image, this defect is clearly detected, although it can be slightly seen also in Fig. 3b, h, j and l. The PPT phasegram (f = 5.7750 Hz – Fig. 3o) allows the detection of the same defects as in Fig. 3a: the wood rings or, strictly speaking, a thermal anomaly, and the two other defects indicated by solid and dotted arrows, having the same colors to facilitate image comparison. The correlation contrast image summarizes the main findings (Fig. 3p) and shows the large thermal anomaly in the bottom of the marquetry, as well as two other defects in the top. For reference, the latter defect indications are surrounded by irregular yellow dotted lines. The corresponding defects seem to be surface, and their presence was confirmed by visual inspection.

Finally, the images obtained by applying thermographic signal reconstruction show the same defect indications found with other processing techniques (Figs. 3 q-s). In particular, these are the defects located at the left hand and the right shoulder of the character, and the one in the bottom of the marquetry (see the arrows in Fig. 3q), as well as the large white spot on the right side (see the arrow in Fig. 3r) and the detachment which is inherent to the tesserae (see the red dotted oval in Fig. 3s). In the latter case, the defect located under the last section of the belt is pointed out with the dotted arrow, as in the case of applying the PCT technique (Figs. 3h, k) and the correlation contrast (Fig. 3p).

The "Girl" sample has been inspected by applying the same processing algorithms, as mentioned above (Fig. 4). The raw IR thermogram (Fig. 4a) reveal the wood rings and some faint thermal anomalies both at the top and at the right side of the sample. The close results have been demonstrated by using the cold image subtraction technique (Fig. 4d). The image of the Fourier magnitude shows some deeper defects marked with the red arrows in Fig. 4b. It is worth noting that detachments are located near the missing parts of the decorative layer (Fig. 2b). The phasegram in Fig. 4b was obtained at the frequency of 0.0250 Hz, and provides an indication of relatively deep features with respect to the shallower defects that can be clearly detected at the higher frequency of 16.7320 Hz in Fig. 4c. In general, the defect indications in Fig. 4c are similar to those in Fig. 4a but the thermal contrast of the wooden rings are better seen in the latter.

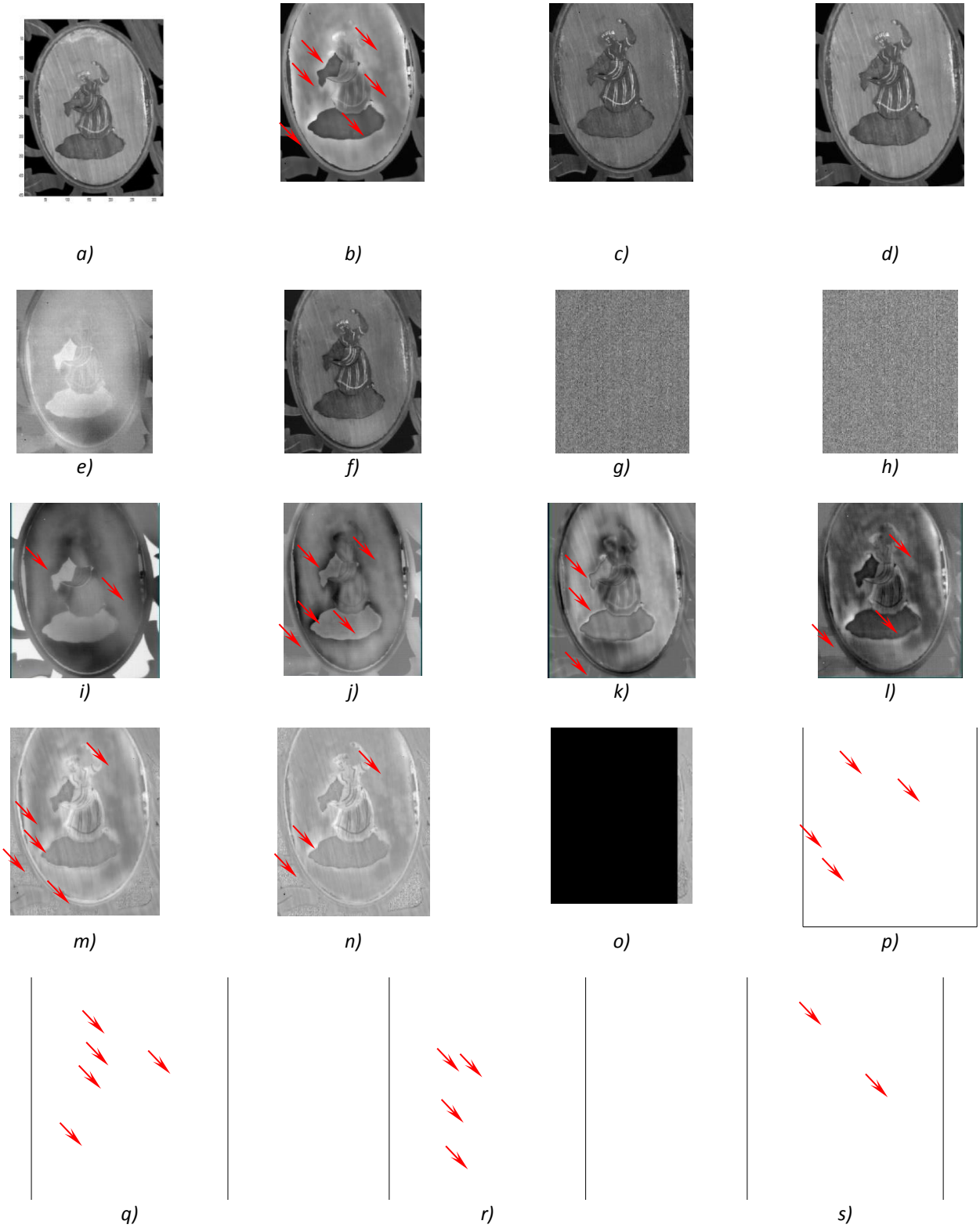

Fig. 4 – "Girl" sample: (a) Raw image (10th frame), (b) Pulse phase Fourier transform amplitude (frame = 2, f = 0.0250 Hz), (c) Pulse phase Fourier transform amplitude (frame = 300, f = 16.7320 Hz), (d) Cold image subtraction contrast (frame = 8), Heating up phase: (e) PC1 – 28.5%, (f) PC2 – 21.4%, (g) PC3 – 7.6%, (h) PC4 – 7.5%, Cooling down phase: (i) PC1 – 12.7%, (j) PC2 – 3.4%, (k) PC3 – 1.3%, (l) PC4 – 0.7%, (m) Pulse phase Fourier transform phase (frame = 4, f = 0.0750 Hz), (n) Pulse phase

Fourier transform phase (frame = 8, *f* = 0.1750 Hz), (o) Pulse phase Fourier transform phase (frame = 26, *f* = 0.6250 Hz), (p) correlation contrast, and Polynomial fitting (order 4): (q) frame 1, (r) frame 2000, (s) frame 500.

The PCT results (Fig. 4e-h) obtained by analysing the heating stage provide no new information about thermal anomalies detected with other processing techniques. In particular, the PC2 image appears similar to that in Fig. 4c obtained by applying the Fourier transform. In their turn, the images in Fig. 4g-h contain only noise thus being useless for defect detection.

More interesting are the images inherent to the processing of the cooling stage of the test procedure (Fig. 4i-l). These results confirm how the most important detachments are located around the object parts with the missing decorative layer (see the red arrows). For example, the PC3 image in Fig. 4k exhibits the indication of a possible defect in the bottom part of the "Girl" sample. In Fig. 4l, it is interesting to notice that the wooden rings are intercalated with spot defects around the half bust of the character. This can be a result of an imperfect adhesion between the support and the *tessellatum* layer by taking into account the anisotropic structure of the wood.

It is known that, when applying the Fourier transform to dynamic temperature signals, images of phase (phasegrams) can be more informative in regard to the corresponding images of magnitude [56]. This is illustrated in Fig. 4m-o. The high-frequency (*f* = 0.6250 Hz) phasegram in Fig. 4o is fairly noisy but the images obtained at *f*=0.0750 Hz (Fig. 4m) and 0.1750 Hz (Fig. 4n) show detachments with the depths from the deeper to the shallower. Respectively, the number of detected defects decreases from Fig. 4m to Fig. 4n. It is interesting to notice that the phasegram clearly reveals the thermal "footprint" of the defect located on the top of the sample (Fig. 4a-d, f). By considering its position, this should appear at *f* = 0.1750 Hz but it is distinctly retrieved by using the correlation contrast (Fig. 4p).

In this case, the technique of polynomial fitting seems to be efficient for detecting hidden structural features [57]. In particular, it seems that the tesserae representing the hair of the character looks detached as seen in Fig. 4q and 4r. The defect at the top of the marquetry is detected in Fig. 4s, while the detachments around the areas with missing wood are visible in all other images.

In the second inspection session, the samples were carefully analysed in order to identify the extension of major defects by the depth (*z*) coordinate.

7. **Testing the** "Boy" and "Girl" samples (square-pulse heating)

In this session, the samples were thermally stimulated for 5 s by means of a 2.5 kW halogen lamp. The temperature distributions were recorded by a FLIR GF309 camera with the acquisition frequency of 15 Hz. Two raw images captured at the end of heating are presented in Fig. 5 to illustrate the non-uniform character of sample thermal patterns.

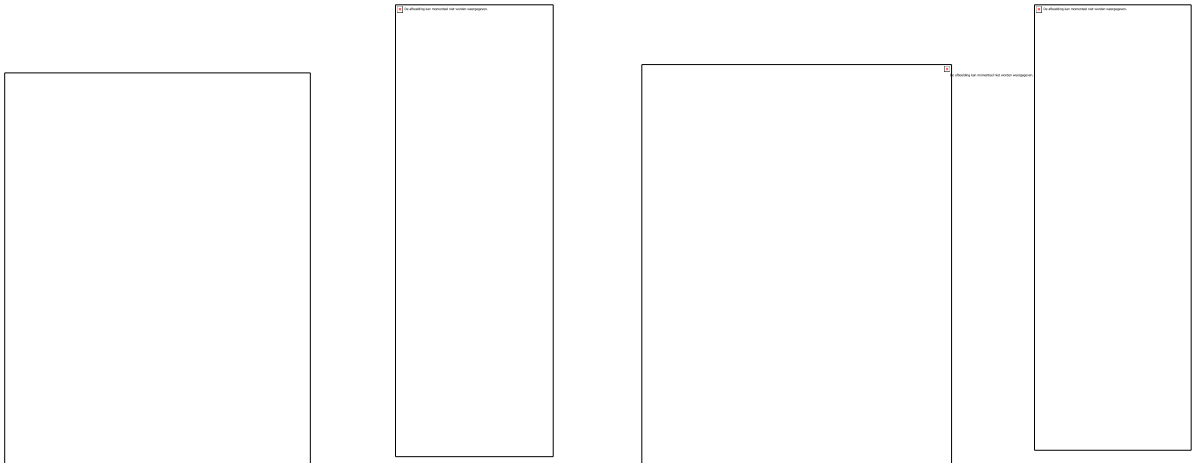

a) *b)*

Fig. 5 – Raw images of the test samples captured at the end of heating: (a) “Boy”, and (b) “Girl”.

Both marquetries exhibit some areas with elevated temperature. For example, the “Boy” sample is characterized by some hot spots in the bottom section, on the right shoulder, on the left hand, on the last part of the belt, and on the left section near the frame. Instead, the “Girl” sample shows thermal anomalies in the upper section, in the right and left sections near the frame, and on the tesserae representing the character hair. The defect indications found in the second experimental section are very similar to those detected earlier. However, it has been expected that a deeper analysis of experimental results may help to detect some more subtle defects.

The images collected at the stage of cooling have been analysed by applying the known technique of PCT [58]. The idea was that different details of the samples should show up in different principal components. This is illustrated in Fig. 6 where principal components reveal differences in sample thickness and colour. The components #1 and #3 mainly characterize the sample surface, while the components #2 and #4 highlight local areas with delaminations (note the 3D appearance of the image of the component #4 where the thickness of the underlined disbond can be clearly followed). Obviously, the sequence of results obtained in the second session by applying a milder thermal stimulus for a longer time should be similar to those obtained with flash heating. A longer heating time is preferable in order to limit the well-known effect of thermochromism [59].

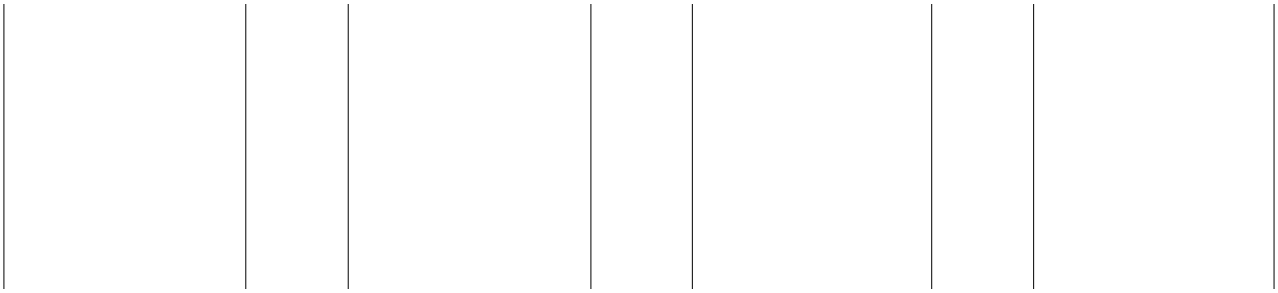

Component #1 *Component #2* *Component #3* *Component #4*

Fig. 6 – Principal component analysis of “Boy” sample.

The same experimental IR image sequences have been processed by applying the DTT technique. Figures 7 and 8 show the sequential thermal tomograms of which in-depth coordinates have been determined by using the corresponding option in Thermo Fit Pro, namely, the known formula $l = \sqrt{a\tau_m}$ (where l is the depth, and a is the diffusivity, for the case of wood a= 8.2×10^{-8} m^2/s). According to this formula, all timegrams contain τ_m values in the range from 0 to 12 s; then, by choosing a particular interval $\tau_{m\,i} \div \tau_{m\,i+1}$, one may separate the $l_i \div l_{i+1}$ layer. For example, the time interval of 4.9÷6.1 s corresponds to the depth interval of 0.4÷0.5 mm. The tomograms Fig. 7,8 clearly show a 3D structure of the marquetry samples with a characteristics in-depth size of some fractions of millimeter. Interpretation of DTT results is not straightforward because of the complicated structure of the samples tested but, for example, it is clearly seen that the thermal anomaly in the left section of the "Boy" sample is mainly located within the 0-0.4 mm layer (Fig. 7). In its turn, the "Girl" sample is thermally inhomogeneous mainly in the 0-0.4 mm layer (Fig. 8). Note that, by introducing an amplitude threshold (30% of the ΔT_m signal in the last image of Fig. 8), one can subdue some minor structural peculiarities to underline some major anomalies.

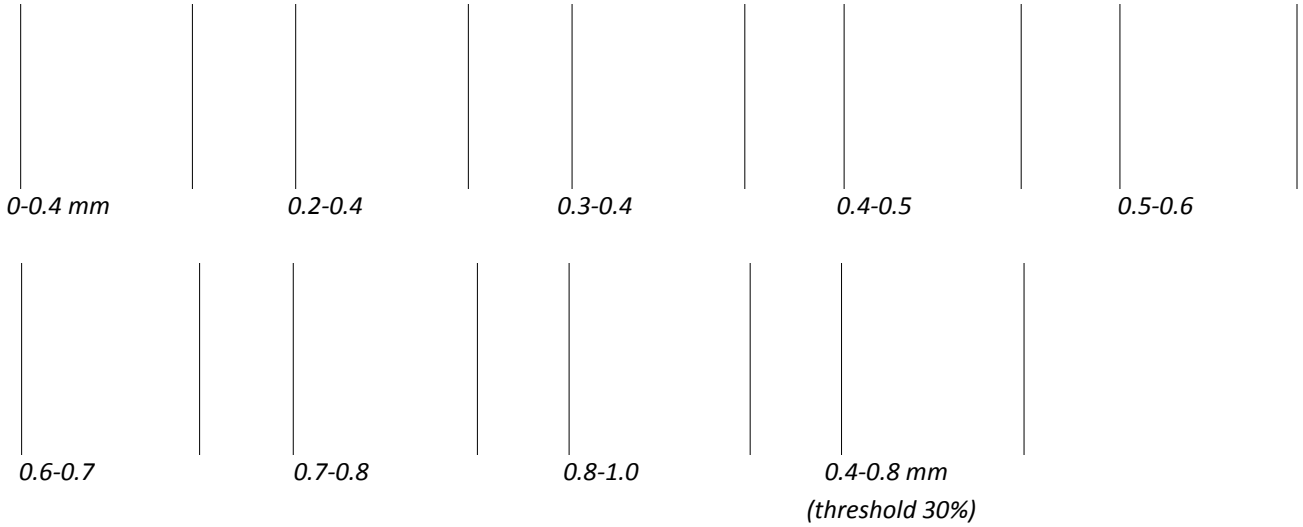

Fig. 7 – Thermal tomograms of "Boy" sample.

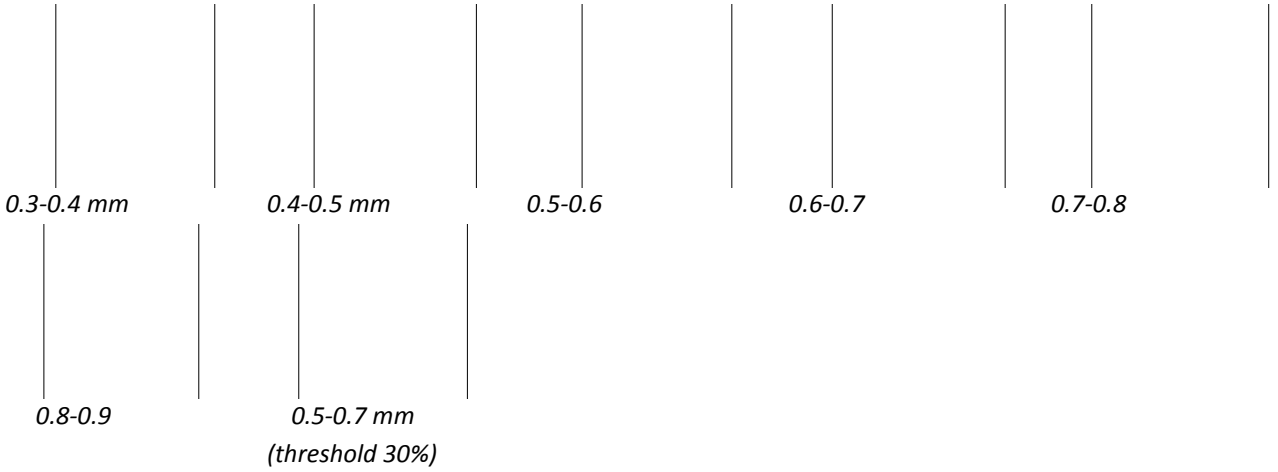

Fig. 8 – Thermal tomograms of “Girl” sample.

8. 1D defect characterization

The one-dimensional (1D) algorithm implemented in ThermoFit Pro® is based on combining the corresponding maxigrams and timegrams values:

$$l = A_1(\alpha, L, \tau_h, K_d) C_m^{\beta_1} \tau_m^{\gamma_1};$$

$$R_d = A_2(\alpha, L, \tau_h, K_d) C_m^{\mu_1} \tau_m^{\sigma_1}, \quad (1)$$

where, are the defect depth [mm] and the thermal resistance [m^2KW^{-1}] respectively, is the material thermal diffusivity, is the sample thickness, is the heating time (heat pulse duration), is the best observation time, is the maximum normalized temperature contrast, and $A_1, A_2, \beta, \gamma, \mu, \sigma$ are the coefficients that depend on the parameters of both a tested material and a test procedure.

The thermal resistance value is related to the defect thickness *d* by the expression:

$$R_d = d/K_{d,} \quad (2)$$

where $K_{d,}$ is the defect thermal conductivity. Therefore, any retrieved R_d value can be matched to the corresponding defect thickness *d* value if K_d is known. However, in many practical cases, K_d is unknown, and the use of the R_d parameter is preferable.

By applying Eq. (1) to the corresponding maxigram and tomogram, one may produce images of defect depth and thermal resistance. The pixel values in such images are expressed in the terms of and (or *d*). Note that accurate results of 1D defect characterization can be obtained only in pulsed one-sided Thermal NDT procedures where pulse duration is arbitrary and all test parameters are properly defined. Also note that quantitative characterization results obtained by means of Eq. (1) adhere to low-conductive (gas-filled) defects only.

The algorithm by Eq. (1) has been applied to the IR image sequences obtained on both the “Boy” and “Girl” samples (Fig. 9). In the “Boy” depth-gram (Fig. 9a), the defect indications show defect depths from 0.49 [mm] in the center to 0.4 [mm] around. The sample thickness-gram (Fig. 9b) showed the defect thermal resistance from

0.003 to 0.005 [m^2KW^{-1}] that corresponded, according to Eq. (2), to defect thickness from 0.2 to 0.3 [mm] if to assume the air conductivity in thin gaps being equal to 0.07 [$W \cdot m^{-1} \cdot K^{-1}$]. Respectively, the "Girl" depth-gram (Fig. 9c) revealed the depth of delamination in the range 0.49-0.51 [mm], while the defect thickness was evaluated to be the same as in the "Boy" sample: 0.2-0.3 [mm] (Fig. 9d).

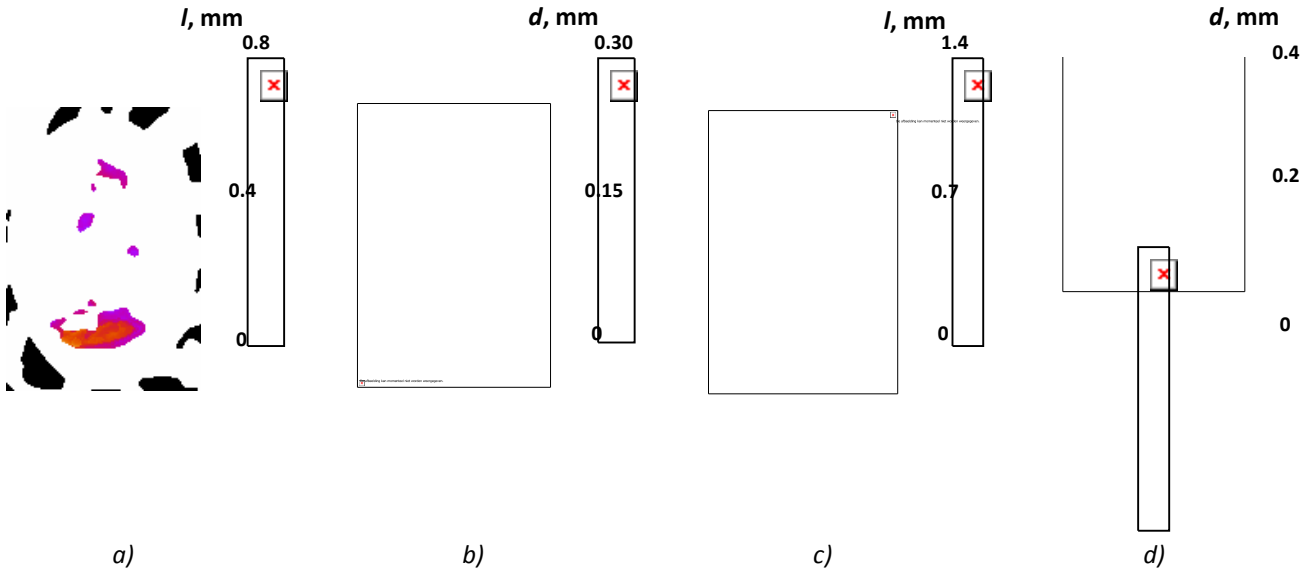

Fig. 9 – Evaluating defect depth and thickness in the “Boy” and “Girl” samples by using the 1D defect characterization algorithm: a – depth-gram (“Boy”), b – thickness-gram (“Boy”), c – depth-gram (“Girl”), d – thickness-gram (“Girl”).

9. Conclusions

In this study, the potential of various TNDT techniques have been demonstrated on two marquetry samples made of fruit woods and having thickness of about 0.5 mm. It should be noted that TNDT has been applied on real artworks containing natural defects. Two sessions of the experimentation have been conducted. The first one involved the mathematical and statistical algorithms intended for the detection of sample thermal anomalies projected on the *x*-*y* plane; after the application of a short thermal stimulus (flash). With this approach, the complete maps of the defects in the “Boy” and “Girl” marquetry samples have been compiled. A special emphasis has been given to the evaluation of defect volume, i.e. estimation of defect depths. The knowledge of these defect parameters is necessary for conducting proper restoration works, for example, by injection of consolidating impregnations. Such defect curing should be performed in a non-destructive way to ensure a perfect continuity between adjacent art object layers.

In this study, the extension of detected thermal anomalies by the in-depth *z*-coordinate has been fulfilled by using the techniques of DTT and 1D defect characterization applied to the results of the second experimental session where long square-pulse heating was applied to the test samples. Thermal tomography resulted in a set of thermal tomograms representing the in-depth sample structure, while the defect characterization algorithm allowed to synthesize images of defect depth (depth-grams) and thickness (thickness-grams).

Since PPT and TSR can also be used to determine the defect depths in case the exact thermal diffusivity values are known, this step is left as future perspective of the present work in order to perform a sort of comparison among the results obtained by all the “volumetric” techniques.

Acknowledgments

This study was supported by the Russian Scientific Foundation grant #19-79-00049 (processing algorithms and test methodology), Russian State Project “Science” 8.13264.2018/8.9 (experimentation) and by Tomsk Polytechnic University Competitiveness Enhancement Program (equipment).

References

[1] Sfarra, S., Yao, Y., Zhang, H., Perilli, S., Scozzafava, M., Avdelidis, N.P., Maldague, X.P.V.: 'Precious walls built in indoor environments inspected numerically and experimentally within long-wave infrared (LWIR) and radio regions', Journal of Thermal Analysis and Calorimetry, 2019, **137**, pp. 1083–1111.

[2] Perilli, S., Sfarra, S., Ambrosini, D., Paoletti, D., Mai, S., Scozzafava, M., Yao, Y.: 'Combined experimental and computational approach for defect detection in precious walls built in indoor environments', International Journal of Thermal Sciences, 2018, **129**, pp. 29–46.

[3] Sfarra, S., Ibarra-Castanedo, C., Paoletti, D., Maldague, X.: 'Infrared vision inspection of cultural heritage objects from the city of L’Aquila, Italy and its surroundings', Materials Evaluation, 2013, **71**, (5), pp. 561–570.

[4] Sfarra, S., Ibarra-Castanedo, C., Tortora, M., Arrizza, L., Cerichelli, G., Nardi, I., Maldague, X.: 'Diagnostics of wall paintings: a smart and reliable approach', Journal of Cultural Heritage, 2016, **18**, pp. 229–241.

[5] Winfree, W.P., James, P.H.: 'Thermographic detection of disbonds'. Proc. of the 35th International Instrumentation Symposium – Instrumentation in the Aerospace Industry (Proceedings of the ISAAerospace Instrumentation Symposium), Orlando (FL), USA, May 1989, Vol. 35, pp. 183–188.

[6] Wu, D., Salerno, A., Sembach, J., Maldague, X.P., Rantala, J.T., Busse, G.: 'Lock-in thermographic inspection of wood particle boards'. Proc. of SPIE – The International Society for Optical Engineering – Thermosense XIX: An International Conference on Thermal Sensing and Imaging Diagnostic Applications, Orlando (FL), USA, April 1997, Vol. 3056, pp. 230–234.

[7] Zhang, H., Sfarra, S., Sarasini, F., Fiorelli, J., Peeters, J., Avdelidis, N.P., Sartori de Lucca, D., Ibarra-Castanedo, C., Perilli, S., Mokhtari, Y., Tirillò, J., Maldague, X.P.V.: 'Impact modelling and a posteriori non-destructive evaluation of homogeneous particleboards of sugarcane bagasse', Journal of Nondestructive Evaluation, 2018, **37**:6, pp. 1–30, DOI: 10.1007/s10921-018-0461-9.

[8] Chulkov, A.O., Sfarra, S., Zhang, H., Osman, A., Szielasko, K., Stumm, C., Sarasini, F., Fiorelli, J., Maldague, X.P.V., Vavilov, V.P.: 'Evaluating thermal properties of sugarcane bagasse-based composites by using active infrared thermography and terahertz imaging', Infrared Physics & Technology, 2019, **97**, pp. 432–439.

[9] Quin Jr., F., Steele, P.H., Shmulsky, R.: 'Locating knots in wood with an infrared detector system', Forest Products Journal, 1998, **48**(10), pp. 80–84.

[10] Nicolotti, G., Miglietta, P.: 'Using high-technology instruments to assess defects in trees', Journal of Arboriculture, 1998, **24**(6), pp. 297–302.

[11] Wyckhuyse, A., Maldague, X.: 'A study of wood inspection by infrared thermography, part I: wood pole inspection by infrared thermography', Research in Nondestructive Evaluation, 2001, **13**(1), pp. 1–12.

[12] Wyckhuyse, A., Maldague, X.: 'A study of wood inspection by infrared thermography, part II: thermography for wood defects detection', Research in Nondestructive Evaluation, 2001, **13**(1), pp. 13–21.

[13] Hwang, G.-S., Hsiung, J.-C., Kuo, M.-Y.: 'Changes in surface temperature of wood specimens during compression testing', Taiwan Journal of Forest Science, 2001, **16**(2), pp. 125–132.

[14] Berglind, H., Dillenz, A.: 'Detection of glue deficiency in laminated wood with pulse thermography', Journal of Wood Science, 2003, **49**(3), pp. 216–220.

[15] Ganne-Chédeville, C., Properzi, M., Pizzi, A., Leban, J.-M., Pichelin, F.: 'Parameters of wood welding: a study with infrared thermography', Holzforschung, 2006, **60**(4), pp. 434–438.

[16] Castellini, P., Abaskin, V., Achimova, E.: 'Portable electronic speckle interferometry device for the damages measurements in veneered wood artworks', Journal of Cultural Heritage, 2008, **9**(3), pp. 225–233.

[17] Ibarra-Castanedo, C., Sfarra, S., Ambrosini, D., Paoletti, D., Bendada, A., Maldague, X.: 'Subsurface defect characterization in artworks by quantitative pulsed phase thermography and holographic interferometry', Quantitative InfraRed Thermography Journal, 2008, **5**(2), pp. 131–149.

[18] Choi, M.Y., Park, J.-H., Kim, W.T., Kang, K.S.: 'Detection of delamination defect inside timber by sonic IR'. Proc. of SPIE – The International Society for Optical Engineering – Thermosense XXX, Orlando (FL), USA, March 2008, Vol. 6939.

[19] Blessley, K., Young, C., Nunn, J., Coddington, J., Shepard, S.: 'The feasibility of flash thermography for the examination and conservation of works of art', Studies in Conservation, 2010, **55**(2), pp. 107–120.

[20] Van Dyk, H., Lemaster, R.L.: 'An investigation of the use of active infrared thermography to detect localized anomalies in lumber', Scanning, 2010, **32**(4), pp. 219–223.

[21] Maierhofer, C., Rollig, M., Krankenhagen, R.: 'Integration of active thermography into the assessment of cultural heritage buildings', Journal of Modern Optics, 2010, **57**(18), pp. 1790–1802.

[22] Sfarra, S., Ibarra-Castanedo, C., Ambrosini, D., Paoletti, D., Bendada, A., Maldague, X.: 'Integrated approach between pulsed thermography, near-infrared reflectography and sandwich holography for wooden panel paintings advanced monitoring', Russian Journal of Nondestructive Testing, 2011, **47**(4), pp. 284–293.

[23] Sfarra, S., Theodorakeas, P., Ibarra-Castanedo, C., Avdelidis, N.P., Paoletti, A., Paoletti, D., Hrissagis, K., Bendada, A., Koui, M., Maldague, X.: 'Evaluation of defects in panel paintings using infrared, optical and ultrasonic techniques', Insight: Non-Destructive Testing and Condition Monitoring, 2012, **54**(1), pp. 21–27.

[24] Sfarra, S., Theodorakeas, P., Avdelidis, N.P., Koui, M.: 'Thermographic, ultrasonic and optical methods: a new dimension in veneered wood diagnostics', Russian Journal of Nondestructive Testing, 2013, **49**(4), pp. 234–250.

[25] Conde, M.J.M., Liñán, C.R., De Hita, P.R., Gálvez, F.P.: 'Infrared thermography applied to wood', Research in Nondestructive Evaluation, 2012, **23**(1), pp. 32–45.

[26] Liñán, C.R., Conde, M.J.M., De Hita, P.R., Gálvez, F.P.: 'Analysis of the influence of density on infrared thermography and of the scope of this technique in the detection of internal defects in wood', Materiales de Construccion, 2012, **62**(305), pp. 99–113.

[27] Mulaveesala, R., Nagarjuna, P., Ravi, D., Amarnath, M.: 'Thermal wave imaging techniques for inspection of plywood materials'. Proc. of SPIE – The International Society for Optical Engineering – Thermosense: Thermal Infrared Applications XXXIV, Baltimore (MD), USA, April 2012, Vol. 8354, Article number 83540C.

[28] Pervan, S., Brezović, M., Prekrat, S., Klarić, M., Sazdevski, G.: 'Possibilities for thermography application in hydrothermal wood processing', Drvna Industrija, 2012, **63**(4), pp. 277–281.

[29] Hoffmann, N., Schröder, T., Schlüter, F., Meinlschmidt, P.: 'Potential of infrared thermography to detect insect stages and defects in young trees', Journal fur Kulturpflanzen, 2013, **65**(9), pp. 337–346.

[30] Morales-Conde, M.J., Rodríguez-Liñán, C., de Hita, R.P.: 'Application of non-destructive techniques in the inspection of the wooden roof of historic buildings: a case study', Advances Materials Research, 2013, **778**, pp. 333–342.

[31] Liñán, C., Morales-Conde, M.J., de Hita, P.R., Gálvez, F.P.: 'Application of non-destructive techniques in the inspection of wooden structures of protected buildings: The case of nuestra señora de los dolores church (Isla Cristina, Huelva)', International Journal of Architectural Heritage, 2015, **9**(3), pp. 324–340.

[32] Keo, S.A., Brachelet, F., Defer, D., Breaban, F.: 'Defects detection by infrared thermography with a new microwave excitation system', Mechanics and Industry, 2014, **15**(6), pp. 509–516.

[33] López, G., Basterra, L.-A., Ramón-Cueto, G., Diego, A.D.: 'Detection of singularities and subsurface defects in wood by infrared thermography', International Journal of Architectural Heritage, 2014, **8**(4), pp. 517–536.

[34] Sfarra, S., Theodorakeas, P., Černeckỳ, J., Pivarčiová, E., Perilli, S., Koui, M.: 'Inspecting marquetries at different wavelengths: the preliminary numerical approach as aid for a wide-range of non-destructive tests', Journal of Nondestructive Evaluation, 2017, **36**(1), Article number 6.

[35] Pahlberg, T., Thurley, M., Popovic, D., Hagman, O.: 'Crack detection in oak flooring lamellae using ultrasound-excited thermography', Infrared Physics and Technology, 2018, **88**, pp. 57–69.

[36] Qiu, Q., Lau, D.: 'Tomography reconstruction methods for damage diagnosis of wood structure in construction field'. Proc. of SPIE – The International Society for Optical Engineering – Nondestructive characterization and monitoring of advanced materials, aerospace, civil infrastructure, and transportation XII, Denver, USA, March 2018, Vol. 10599, Article number 1059915.

[37] Garrido, I., Lagüela, S., Sfarra, S., Madruga, F.J., Arias, P.: 'Automatic detection of moistures in different construction materials from thermographic images', Journal of Thermal Analysis and Calorimetry, 2019, Journal of Thermal Analysis and Calorimetry, 2019, **138**(2), pp. 1649–1668.

[38] Laureti, S., Sfarra, S., Malekmohammadi, H., Burrascano, P., Hutchins, D.A., Senni, L., Silipigni, G., Maldague, X.P.V., Ricci, M.: 'The use of pulse-compression thermography for detecting defects in paintings', NDT and Evaluation International, 2018, **98**, pp. 147–154.

[39] Yao, Y., Sfarra, S., Lagüela, S., Ibarra-Castanedo, C., Wu, J.-Y., Maldague, X.P.V., Ambrosini, D.: 'Active thermography testing and data analysis for the state of conservation of panel paintings', International Journal of Thermal Sciences, 2018, **126**, pp. 143–151.

[40] Peeters, J., Van der Snickt, G., Sfarra, S., Legrand, S., Ibarra-Castanedo, C., Janssens, K., Steenackers, G.: 'IR reflectography and active thermography on artworks: the added value of the 1.5 – 3 μm band', Applied Sciences, 2018, **8**(1), Article number 50.

[41] Sfarra, S., Fernandes, H.C., López, F., Ibarra-Castanedo, C., Zhang, H., Maldague, X.: 'Qualitative assessments via infrared vision of sub-surface defects present beneath decorative surface coatings', International Journal of Thermophysics, 2018, **39**(1), Article number 13.

[42] Scudieri, F., Mercuri, F., Volterri, R.: 'Non-invasive analysis of artistic heritage and archaeological findings by time resolved IR thermography', Journal of Thermal Analysis and Calorimetry, 2001, **66**(1), pp. 307–314.

[43] Mercuri, F., Zammit, U., Orazi, N., Paoloni, S., Marinelli, M., Scudieri, F.: 'Active infrared thermography applied to the investigation of art and historic artefacts', Journal of Thermal Analysis and Calorimetry, 2011, **104**, pp. 475–485.

[44] Androsch, R., Pyda, M., Wang, H., Wunderlich, B.: 'A study of temperature-modulated differential scanning calorimetry with high-resolution infrared thermography', Journal of Thermal Analysis and Calorimetry, 2000, **61**(3), pp. 661–679.

[45] Yousefi, B., Sfarra, S., Ibarra-Castanedo, C., Avdelidis, N.P., Maldague, X.P.V.: 'Thermography data fusion and nonnegative matrix factorization for the evaluation of cultural heritage objects and buildings', Journal of Thermal Analysis and Calorimetry, 2019, **136**(2), pp. 943–955.

[46] Vargas Aparicio, J.H., Ortega Arroyo, L., Mollinedo Ponce de León, H.R., Ortega Herrera, J.Á., Rodríguez Arias, Y.A., Arellano González, S., Rodríguez-Romo, S., M. Castaño, V.: 'Implementation of the boundary element method for detecting defects by transient thermography on an aluminium plate', Journal of Thermal Analysis and Calorimetry, 2016, **126**(2), pp. 671–679.

[47] Yao, Y., Sfarra, S., Ibarra-Castanedo, C., You, R., Maldague, X.P.V.: 'The multi-dimensional ensemble empirical mode decomposition (MEEMD): ad advanced tool for the thermographic diagnosis of mosaics', Journal of Thermal Analysis and Calorimetry, 2017, **128**(3), pp. 1841–1858.

[48] Sfarra, S., Perilli, S., Paoletti, D., Ambrosini, D.: 'Ceramics and defects. Infrared thermography and numerical simulations – a wide-ranging view for quantitative analysis', Journal of Thermal Analysis and Calorimetry, 2016, **123**(1), pp. 43–62.

[49] Sfarra, S., Regi, M., Tortora, M., Casieri, C., Perilli, S., Paoletti, D.: 'A multi-technique non-destructive approach for characterizing the state of conservation of ancient bookbindings', Journal of Thermal Analysis and Calorimetry, 2018, **132**(2), pp. 1367–1387.

[50] Tavakolian, P., Sfarra, S., Gargiulo, G., Sivagurunathan, K., Mandelis, A.: 'Photothermal coherence tomography for 3-D visualization and structural non-destructive imaging of a wood inlay', Infrared Physics and Technology, 2018, **91**, pp. 206–213.

[51] Edwards, C.: '"Improving" the decoration of furniture: imitation and mechanization in the marquetry process in Britain and America, 1850-1900', Technology and Culture, 2012, **53**(2), pp. 401–434.

[52] Klein, M.T., Ibarra-Castanedo, C., Maldague, X.P., Bendada, A.: 'A straightforward graphical user interface for basic and advanced signal processing of thermographic infrared sequences'. Proc. of SPIE – The International Society for Optical Engineering – Thermosense: Thermal Infrared Applications XXX, Orlando (FL), USA, March 2008, Vol. 6939, Article number 693914.

[53] Vavilov, V.P.: 'Dynamic thermal tomography: recent improvements and applications', NDT&E International, 2015, **71**, pp. 23–32.

[54] Vavilov, V.P., Maldague, X., Dufort, B., Robitaille, J., Picard, J.: 'Thermal NDT of carbon epoxy composites: detailed analysis and data processing', NDT&E International, 1993, **26**(2), pp. 85–95.

[55] Vavilov, V.P., Grinzato, E., Bison, P.G., Marinetti, S., Bressan, C.: 'Thermal characterization and tomography of carbon fiber reinforced plastics using individual identification technique', Materials Evaluation, 1996, **54**(5), pp. 604–610.

[56] Maldague, X., Marinetti, S.: 'Pulse phase infrared thermography', Journal of Applied Physics, 1996, **79**(5), 2694.

[57] Shepard, S.M., Lhota, J.R., Rubadeux, B.A., Wang, D., Ahmed, T.: 'Reconstruction and enhancement of active thermographic image sequences', Optical Engineering, 2003, **42**(5), 1337-1342.

[58] Rajic, N.: 'Principal component thermography for flaw contrast enhancement and flaw depth characterisation in composite structures', Compos. Struct., 2002, **58**, 521-528.

[59] Seeboth, A., Lötzsch, D. 'Thermochromic and thermotropic materials', 1st ed.; Jenny Standford Publishing (Taylor & Francis Group): U.S.A., Boca Raton (FL), 2013; pp. 1–228.